Int. J. Heat Mass Transfer. Vol. 31, No. 8, pp. 1735–1744, 1988
Printed in Great Britain

0017–9310/88 $3.00 + 0.00

Solidification of a pure metal at a vertical wall in the presence of liquid superheat

F. WOLFF and R. VISKANTA
Heat Transfer Laboratory, School of Mechanical Engineering, Purdue University, West Lafayette, IN 47907, U.S.A.

(*Received* 3 *November* 1987 *and in final form* 9 *February* 1988)

Abstract—The role of natural convection during solidification of a pure metal at a vertical wall is studied experimentally and numerically. Experiments are performed in a rectangular test cell with two opposing sidewalls held at constant but different temperatures, while the remaining walls are well insulated. Pure tin is used as the phase-change material. Temperature and solid–liquid interface position measurements made under carefully controlled conditions are employed to deduce the importance of natural convection in the liquid metal on the temperature distribution in the melt as well as on the shape and motion of the solid–liquid interface. The experimental data are compared with results of a numerical prediction.

INTRODUCTION

OWING to the interest in solidification conditions necessary to eliminate macrosegregation and intercellular segregation in metals or semiconductors, the influence of natural convection on the solidification processes has received considerable research interest during the last two decades [1]. Materials processing, purification of metals and continuous casting are just a few applications motivating research in this area. However, a review of the heat transfer and metallurgical literature shows that solidification rate data, in the presence of liquid superheat, have seldom been acquired under carefully controlled boundary conditions [2]. Only recently, interface locations as well as temperature distributions have been accurately determined.

The effects of laminar, thermally driven natural convection on the shape and the motion of the solid–liquid interface during the controlled solidification of pure metals has been investigated both experimentally and theoretically [3, 4]. More recently, experimental results for solidification of gallium on a vertical wall of a rectangular cavity were reported in ref. [2]. Due to the anisotropy in the thermal conductivity of gallium and crystallographic effects, the interface is found to be highly irregular. Vives and Perry [5, 6] experimentally investigated the influence of magnetically induced forced convection as well as thermally and solutally driven natural convection during solidification of metals and alloys and related the heat transfer data to metallurgical findings.

To the authors' knowledge, Ramachandran *et al.* [7] are the only ones who presented a two-dimensional numerical model of solidification in a rectangular cavity with superheat present in the liquid. Numerical calculations have been performed for several relevant dimensionless parameters, but the lowest Prandtl number considered is $Pr = 0.1$, which is one order of magnitude higher than the Prandtl number of most metals. No comparison of experimental data with predictions of a two-dimensional numerical model, simulating solidification of a superheated metal in a rectangular cavity, have been identified in the relevant literature, even though such information is of considerable practical importance [8, 9].

As evident from the literature review, solidification of low Prandtl number liquids has not received adequate research attention. Hence, the purpose of this paper is to report on experiments concerned with the solidification of superheated tin (99.99% pure) at a vertical wall under carefully controlled conditions. Experiments are performed in a rectangular cavity. Two vertical sidewalls of the test cell are held at constant but different temperatures, while the connecting top and bottom walls as well as the front and backwalls are well insulated. Tin is selected as the working fluid because its thermophysical properties are reasonably well documented [10, 11], and its fusion temperature is low in comparison to other metals. Temperature and interface position measurements are employed to deduce the importance of natural convection in the melt on the solidification process. In addition, the experimental data are compared to results of a numerically simulated experiment. The velocity vector maps predicted by the numerical model serve to visualize the complicated flow structure.

EXPERIMENTS

Apparatus and instrumentation

The experiments are performed in a rectangular cavity with two vertical sidewalls held at constant but different temperatures. The remaining walls of the cavity are well insulated. Figure 1 shows the principal features of the experimental apparatus. The test cell is constructed from a commercially available five-sided Pyrex glass tank with 7 mm thick walls. Since the

NOMENCLATURE

A	aspect ratio, H/W
g	gravitational acceleration
c	specific heat of the phase-change material
Fo	Fourier number, $\alpha_l t/W^2$
H	height of the cavity
Δh_f	latent heat of fusion
P	pressure
Pr	Prandtl number, ν/α
Ra	Rayleigh number, $g\beta(T_H - T_f)W^3/\alpha\nu$
s	solid–liquid interface position
Ste	Stefan number, $c(T_f - T_C)/\Delta h_f$
T	temperature
t	time
u	velocity in the x-direction
V	solidified volume
V_0	total volume of the test cavity
v	velocity in the y-direction
W	width of the cavity
x	coordinate direction parallel to the heat exchangers (Fig. 3)
y	coordinate direction normal to the heat exchangers (Fig. 3).

Greek symbols

α	thermal diffusivity
β	thermal expansion coefficient
θ	dimensionless temperature in the liquid, $(T_l - T_f)/(T_H - T_f)$
ν	kinematic viscosity
τ	dimensionless time, $Ste\,Fo$.

Subscripts

C	cold
f	fusion
H	hot
i	initial
l	liquid.

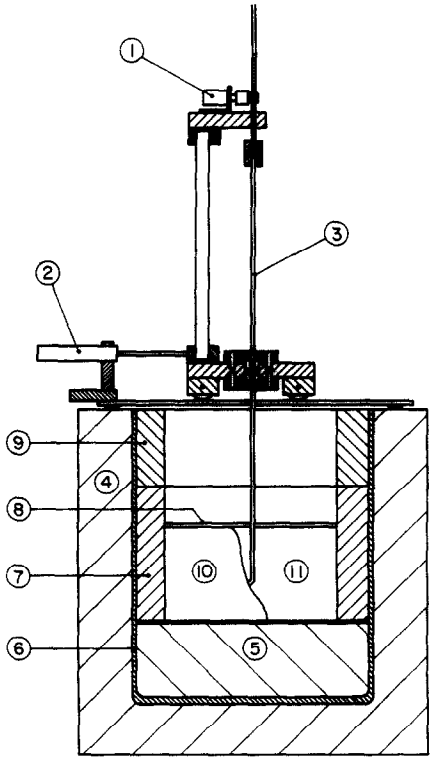

FIG. 1. Schematic of the experimental apparatus: 1, ten-turn potentiometer; 2, linear potentiometer; 3, probe; 4, Sylox 2 μm sized silica; 5, sand; 6, five-sided glass tank; 7, heat exchangers; 8, 75 mm lava plate; 9, 5 mm lava plate; 10, solid; 11, liquid.

vertical extent of the tank is larger than the desired height of the test section, the bottom of the tank is partially filled with sand. A 5 mm thick Pyrex glass plate is placed on the sand to separate the test region from the sand. Two heat exchangers, which serve as the heat source/sink, are then inserted into the tank and fixed on two opposite vertical walls. The glass plate at the bottom, two vertical walls of the glass tank and the two heat exchangers form the bottom and the sidewalls of the test region, respectively. A 5 mm thick lava plate, serving as the top boundary of the test region, is placed on the tin. Another 75 mm thick lava plate is situated on top of the heat exchangers. Between the two lava plates is an air gap the thickness of which varies with the aspect ratio. The configuration allows flexibility to vary the aspect ratio and provides good insulation at the top. Slots are milled into both lava plates to insert probes from the top.

The actual test region is 8.89 cm wide and 12.6 cm deep. The height is 6.66 or 8.89 cm depending on the desired aspect ratio (0.75 or 1.0). The entire glass tank is placed in a wooden box which is 8 cm larger than the tank at all four sides and at the bottom. The space between the wooden box and the glass tank is filled with Sylox 2 μm sized silica, an extremely good insulator ($k = 0.02\ \mathrm{W\,m^{-1}\,K^{-1}}$).

Each of the two heat exchangers consists of a 10 mm thick copper plate, five electric resistance heaters and a multipass heat exchanger machined from a 15 mm thick brass plate (Fig. 2). The copper plate is in direct contact with the test material. The heaters are attached to the back side of the copper plate. Each heater is made out of two 2.54 mm thick high thermal conductivity boron nitride plates ($k = 65\ \mathrm{W\,m^{-1}\,K^{-1}}$) and a 0.35 mm diameter nickel–chromium resistance wire. In the plate, which is in direct contact with the copper plate, 0.5 mm deep grooves are milled. The nickel–chromium wire is laid into the grooves and the other boron nitride plate is placed on top of the grooved plate. The temperatures of each individual heater are measured with either one or two type-K

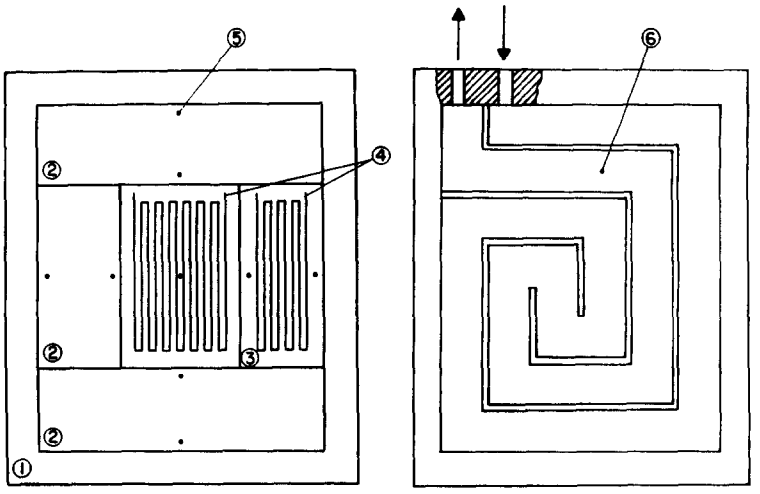

FIG. 2. Schematic diagram of the heat exchanger: 1, copper block; 2, heater (assembled); 3, grooved boron nitride plate (top plate of the heater removed); 4, nickel–chromium wire; 5, thermocouple locations; 6, multipass heat exchanger.

thermocouples which are located in the copper plate at a distance of 0.02 mm from the surface adjacent to the tin. The copper plate and the five heaters serve as a top plate for the channels of the multipass heat exchanger. This construction provides the possibility for both, heating and cooling. If the heat source/sink is used as a heater, no fluid is circulated through the channels, while there is electric power input into the heater. If the unit serves as a sink, air is circulated through the channels and heat is removed from the heat sink. During cooling the heaters are employed to equalize temperature nonuniformities along the copper plate. In both cases, a HP Model-3852 data logger is used to control the electric power input into the heaters so as to achieve a uniform temperature over the entire heat exchanger surface. This is accomplished by comparing the measured temperatures at the copper plate surface with the temperature desired as the boundary condition. Based on this comparison, the relay of each individual heater is either opened or closed. The air flow rate through the heat exchanger is manually controlled. With this heat exchanger design and due to the relatively small temperature differences between the heat exchangers, the temperature nonuniformities along each copper plate are reduced to $\pm 0.1°C$.

Temperature profiles in the liquid tin and positions of the solid–liquid interface are measured with a movable thermocouple probe and a movable L-shaped glass rod, respectively. In order to determine the location of the probes, an x–y measurement system is developed which consists of a rectangular frame and a cart. The frame, fixed on top of the wooden box, has rails on two opposite sides, serving as guideways for the wheels of the cart. The position of the cart and thus the horizontal location of the probe is determined with a linear potentiometer, attached to the cart and fixed to the frame. The vertical position of the probe is measured with a ten-turn potentiometer which is installed on the cart. A gear on the shaft of the ten-turn potentiometer grips a precision rack connected to the probe. When the probe is moved up and down, the rack induces a rotation at the ten-turn potentiometer. The resulting electrical signals from both potentiometers are fed into the data logger. It is estimated that the position of the probe can be determined with an accuracy of ± 1 mm.

The temperature probe consists of a type-K thermocouple wire inserted into a 3 mm outer diameter glass tube. For protection purposes, the thermocouple bead at the tip of the rod is coated with a thin layer of high thermal conductivity epoxy. The thermocouple is calibrated against the freezing point of tin with an accuracy of $\pm 0.1°C$.

Experimental procedure and data reduction

The test material used in the experiments is 99.99% pure tin with a melting point of 231.9°C. The thermophysical properties of tin are obtained from the literature [10, 11].

Before solidification is started, the temperatures of both heaters are maintained at the initial values above the fusion temperature of tin for at least 6 h. The phase-change process is initiated by lowering the temperature of one of the heat exchangers below the fusion temperature of tin, while the other one is kept at the initial temperature above the fusion temperature of tin. In order to assure measurements under quasi-steady-state conditions, the temperature differences between the two heat exchangers are kept small, so that the interface moves only a small distance while data are taken.

The probing method is used to determine the position of the interface at preselected times after the initiation of phase change. An L-shaped rod is immersed into the liquid metal and is moved along

the solid–liquid interface. The position of the tip of the glass rod, which is in direct contact with the interface, is measured with the x–y measurement system at discrete points. The error resulting from the deflection of the probe tip, due to bending of the glass rod during measurements, is predetermined and minimized by reducing the contact pressure between the tip of the probe and the interface. Temperature data at preselected times, which correspond in time to the interface position data, are obtained by performing another experiment under the identical boundary and initial conditions for which the interface position data are taken. The temperatures in the melt are measured at three different heights by traversing the probe horizontally through the liquid metal, against the assumed direction of the flow, in order to minimize the disturbance of the flow and temperature fields by the previous measurements.

All temperature and interface data are taken at the centerplane of the test cell. The interface position data are only obtained at preselected times so that the disturbance of the flow and temperature fields by the measurements does not significantly influence the solidification process. Small temperature differences (of the order of 1–4°C) were imposed between the cold (T_C) and hot (T_H) walls of the test cell. This was done in order to reduce the motion of the solidification front during the time it takes to locate the interface position.

ANALYSIS

Two-dimensional solidification in a rectangular enclosure with superheat in the melt is mathematically modeled by Ramachandran *et al.* [7]. In order to take advantage of the numerical algorithm to simulate solidification of pure tin at a vertical isothermal wall, while the opposite wall was maintained at the initial temperature above the fusion temperature of tin, the boundary conditions at one vertical side of the computational domain was changed. A vertical centerplane symmetry boundary condition was replaced by a constant wall temperature boundary condition. A schematic of the physical model and the coordinate system used in the present work is shown in Fig. 3. The following assumptions are made:

(1) the thermophysical properties of the phase-change material in the solid and liquid state are independent of temperature, with the exception of the density in the buoyancy term in the momentum equations;

(2) the Boussinesq approximation is valid;

(3) the flow in the melt is incompressible, laminar and two-dimensional;

(4) the melt is a Newtonian fluid;

(5) the model does not account for finite velocities at the solid–liquid interface due to the volume change of the material during solidification.

With these assumptions, the conservation equations of mass, momentum and energy in the melt and the energy conservation equation in the solid can be written, respectively, as:

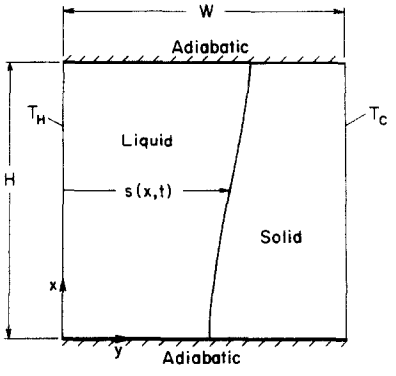

FIG. 3. Schematic of the physical model and coordinate system.

continuity

$$\frac{\partial u}{\partial x}+\frac{\partial v}{\partial y}=0; \tag{1}$$

momentum in the x-direction

$$\frac{\partial u}{\partial t}+u\frac{\partial u}{\partial x}+v\frac{\partial u}{\partial y}=-\frac{1}{\rho}\frac{\partial P}{\partial x}+g\beta(T_l-T_f)+\nu\left(\frac{\partial^2 u}{\partial x^2}+\frac{\partial^2 u}{\partial y^2}\right); \tag{2}$$

momentum in the y-direction

$$\frac{\partial v}{\partial t}+u\frac{\partial v}{\partial x}+v\frac{\partial v}{\partial y}=-\frac{1}{\rho}\frac{\partial P}{\partial y}+\nu\left(\frac{\partial^2 v}{\partial x^2}+\frac{\partial^2 v}{\partial y^2}\right); \tag{3}$$

energy in the melt

$$\frac{\partial T_l}{\partial t}+u\frac{\partial T_l}{\partial x}+v\frac{\partial T_l}{\partial y}=\alpha_l\left(\frac{\partial^2 T_l}{\partial x^2}+\frac{\partial^2 T_l}{\partial y^2}\right); \tag{4}$$

energy in the solid

$$\frac{\partial T_s}{\partial t}=\alpha_s\left(\frac{\partial^2 T_s}{\partial x^2}+\frac{\partial^2 T_s}{\partial y^2}\right); \tag{5}$$

the initial and boundary conditions in the melt

$T_l = T_i$; $u = v = 0$ for $t = 0$

$T_l = T_f$; $u = 0$; $v = 0$ at the solid–liquid interface, $s = F(x, t)$

$T_l = T_H$; $u = 0$; $v = 0$ at the hot wall, $y = 0$

$\dfrac{\partial T_l}{\partial x} = 0$; $u = 0$; $v = 0$ at top and bottom connecting walls, $x = 0$ and H, $0 \leqslant y \leqslant s$. (6)

An energy balance at the solid–liquid interface yields

$$\rho\Delta h_f\frac{\partial s}{\partial t}=\left(1+\left(\frac{\partial s}{\partial x}\right)^2\right)\left(k_s\frac{\partial T_s}{\partial x}-k_l\frac{\partial T_l}{\partial y}\right). \tag{7}$$

The boundary conditions in the solid are

$T_s = T_f$ at the solid–liquid interface, $s = F(x, t)$

$T_s = T_C$ at the cold wall, $y = W$

$\frac{\partial T_s}{\partial x} = 0$ at top and bottom connecting walls

$x = 0$ and H, $s < y \leqslant W$. (8)

The governing equations were nondimensionalized and discretized using a finite-difference technique. The computational domain encompassed the melt and the solid and 31×31 control volumes were employed in each of these regions. The details of the numerical procedure are given elsewhere [7] and are not repeated here.

Tests of the accuracy of the numerical algorithm were performed. The thickness of the solid layer at early times was compared with Neumann's solution [12], and the predicted results agreed to within 0.1% of the exact solution. Nusselt numbers obtained along the two vertical sidewalls were compared with benchmark solutions for steady-state natural convection of air in a square cavity [13]. The agreement was found to better than 2% for $Ra \leqslant 10^4$ and better than 8% for $Ra \leqslant 10^6$. The discrepancies are attributed to the relatively coarse, equally distributed grid and the transient terms in the governing equations which cannot be completely eliminated in the present numerical procedure.

RESULTS AND DISCUSSION

Interface shape and position

The progression of the solid–liquid interface with time for three different temperature differences $(T_H - T_C)$ is shown in Figs. 4–6. At early times, the solid–liquid interface is only slightly curved, indicating that heat transfer is predominantly by conduction. As time progresses, buoyancy driven natural convection in the liquid metal influences the local heat transfer rate at the solid–liquid interface. The curved interfaces provide conclusive evidence of this effect. The fluid in the vicinity of the hot plate rises and its temperature increases as it flows along the heat exchanger. When the liquid tin reaches the top of the melt layer, it turns 90° and impinges at the solid–liquid interface. The flow is deflected and descends along the interface while its temperature decreases. Due to the higher temperature of the liquid metal near the top of the solid–liquid interface, the local solidification rate is lowest in this region. By the time the liquid has reached the lower part of the melt filled cavity, it has been cooled down to nearly its fusion temperature. The melt turns 90° and flows back towards the hot wall. Since the heat transfer rate from the hot wall to the interface by conduction is reduced by the advective energy transport, the solidification rate at the lower part of the interface is higher than one would expect for pure conduction.

Figures 4 and 5 depict the progression of the interface at preselected times for two different cold-wall temperatures. While the contours of the interfaces at

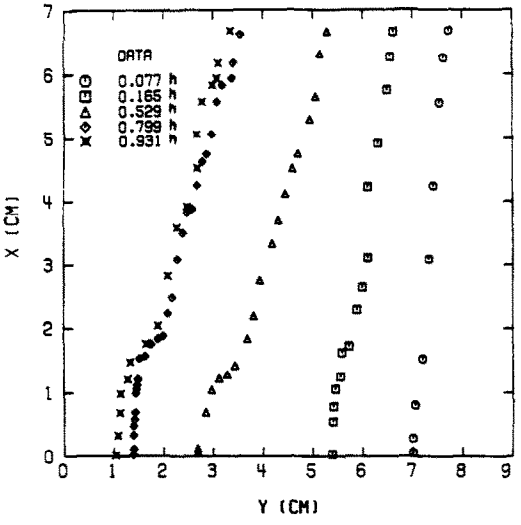

FIG. 4. Interface shape taken at preselected times: $T_i = 233.0°C$, $T_H = 233.0°C$, $T_C = 226.0°C$, $A = 0.75$, $Ra = 1.59 \times 10^5$, $Ste = 2.69 \times 10^{-2}$.

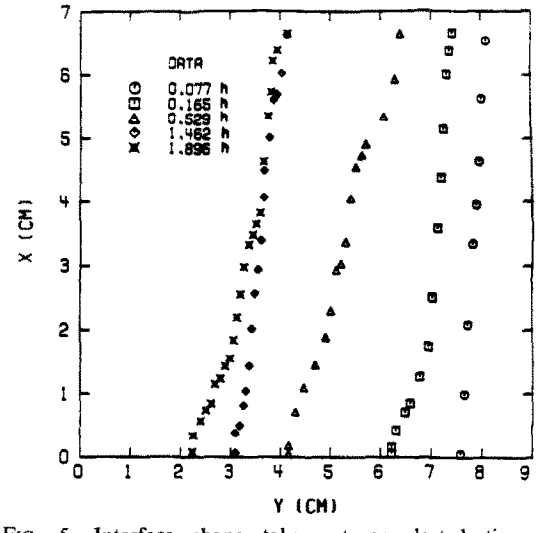

FIG. 5. Interface shape taken at preselected times: $T_i = 233.0°C$, $T_H = 233.0°C$, $T_C = 229.0°C$, $A = 0.75$, $Ra = 1.59 \times 10^5$, $Ste = 1.32 \times 10^{-2}$.

the same time increment are only slightly different, the solidification rate decreases with increasing temperatures at the cold wall. For lower cold-wall temperatures (Fig. 4), the steady-state interface position is reached after a shorter time period than for higher cold-wall temperatures (Fig. 5).

A comparison of Figs. 4 and 6 shows the influence of initial superheat in the liquid metal and hot-wall temperature on the position and the shape of the solid–liquid interface. For increasing superheat and hot-wall temperature, the nonuniformities in the interface shape are more pronounced which can be attributed to an intensification of the flow in the melt. In case of higher superheat and hot-wall temperature (Fig. 6), the progression of the interface is slower and the solidified volume at steady state is smaller than in

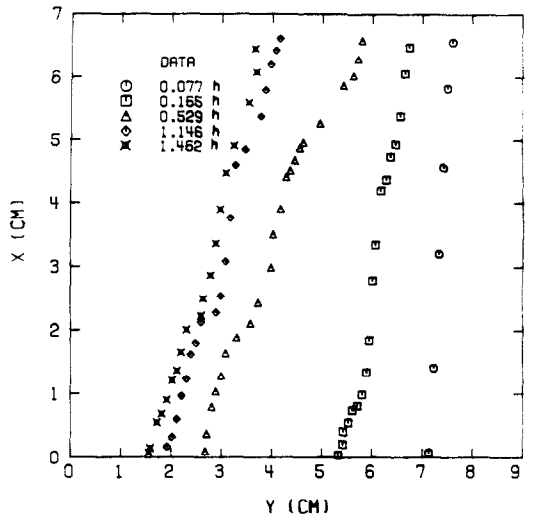

FIG. 6. Interface shape taken at preselected times: $T_i = 234.0°C$, $T_H = 234.0°C$, $T_C = 226°.0°C$, $A = 0.75$, $Ra = 3.01 \times 10^5$, $Ste = 2.69 \times 10^{-2}$.

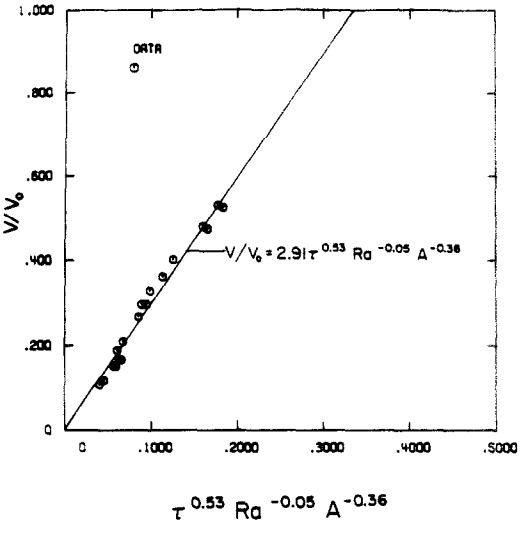

FIG. 7. Correlation of the solidified volume fraction data.

the case of lower superheat and hot-wall temperature (Fig. 4), because of a higher heat transfer rate from the liquid pool to the interface.

Even though heat losses from the front- and back-walls of the test cell to the ambient occur, an increased solidification rate in these locations and thus a curvature of the solid–liquid interface in the direction parallel to the two heat exchangers is not observed. This can be explained by the fact that the heat removal at the cold wall is much higher than the heat losses from the front- and backwalls of the test cell to the ambient.

The variation of the solidified volume fraction with time is determined by integrating the interface contour. The data are depicted in Fig. 7. The best curve fit could be achieved by using non-linear regression and employing dimensionless time (τ), Rayleigh number (Ra) and aspect ratio (A) as the dimensionless parameters (see Nomenclature). The experimental data collapse quite well onto a single curve if V/V_0 is used as an ordinate and $\tau^{0.53} Ra^{-0.05} A^{-0.36}$ as an abscissa. The correlation

$$V/V_0 = 2.91\tau^{0.53} Ra^{-0.05} A^{-0.36} \quad (9)$$

is shown as a solid line in Fig. 7. The correlation is restricted to $\tau \leqslant 0.1076$, because for $\tau > 0.1076$ the solidification process approaches steady state (i.e. the solidified volume does not increase with time), while in the correlation a time dependence of the solidified volume is assumed. The exponent of the dimensionless time τ of 0.53 is close to the exponent found for pure conduction solution, $V/V_0 \propto \tau^{0.5}$ [12]. The Rayleigh number as well as the aspect ratio have negative exponents, indicating that the solidified volume fraction decreases with increasing Rayleigh numbers and aspect ratios. These findings are consistent with the results for steady-state natural convection of liquid metals [14] which show increasing heat transfer rates with increasing aspect ratios and Rayleigh numbers.

Heat transfer characteristics

Temperature profiles measured at three different heights in the liquid tin and two preselected times are depicted in Figs. 8 and 9. The temperature data in Figs. 8 and 9 correspond to the interface locations at $t = 0.077$ and 0.529 h in Fig. 5, respectively. At early times, temperature profiles typical of natural convection in a rectangular enclosure are observed. The convective flow causes steep temperature gradients at the hot wall and the solid–liquid interface. Along the interface, the temperature gradients are high in the upper region of the cavity and decrease towards the bottom. The opposite trend is evident at the heated wall. The trends of the measured liquid temperatures are consistent with the clockwise circulation of the melt. While local heat transfer from the liquid to the solid–liquid interface varies with height, the interface remains nearly planar (Fig. 5), owing to the dominance of heat conduction in the solid layer over convective energy transport in the liquid.

At $t = 0.529$ h (Fig. 9) again, temperature profiles typical of natural convection in a rectangular cavity are observed. Due to the increasing thermal resistance of the solid layer and thus reduced heat conduction from the interface to the chilled plate, heat transfer from the liquid pool to the solid–liquid interface by convection plays an important role in the local energy balance at the interface. The curved solidification front provides conclusive evidence of this phenomenon.

The scatter of the experimental temperature data may be due to several reasons. First, the immersion of a thermocouple probe into a liquid metal undergoing natural convection is believed to cause the onset of temperature oscillations [1]. Second, the on–off control employed to control the heat exchanger tem-

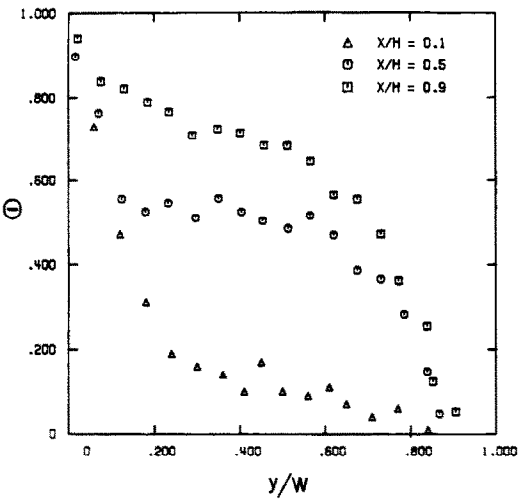

FIG. 8. Temperature distributions in the liquid at three different heights: $T_i = 233.0°C$, $T_H = 233.0°C$, $T_C = 229.0°C$, $A = 0.75$, $Ra = 1.59 \times 10^5$, $Ste = 1.32 \times 10^{-2}$, $t = 0.079$h ($Fo = 0.63$).

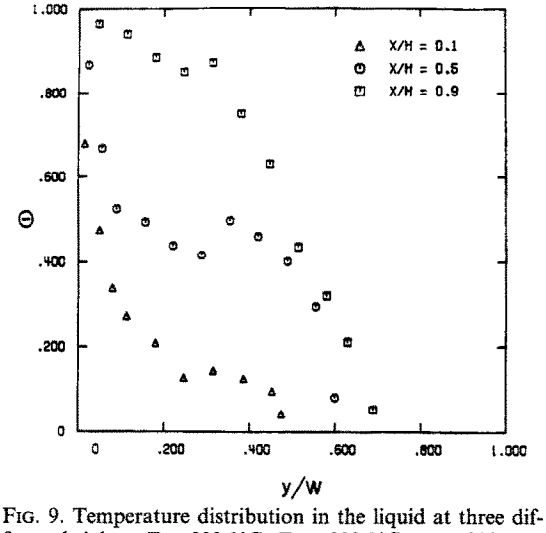

FIG. 9. Temperature distribution in the liquid at three different heights: $T_i = 233.0°C$, $T_H = 233.0°C$, $T_C = 229.0°C$, $A = 0.75$, $Ra = 1.59 \times 10^5$, $Ste = 1.32 \times 10^{-2}$, $t = 0.529$ h ($Fo = 4.31$).

peratures produces oscillations in the system. Third, the motion of the solid–liquid interface and thus the decrease in the size of the melt region produces unsteady fluid flow [2] and may, in turn, produce oscillations in the temperature. Fourth, the difficulty of wetting the metallic thermocouple by liquid tin may have contributed to the scatter. Finally, the thermocouples are only accurate to within $\pm 0.1°C$, and the scatter of the data may be explained by the uncertainty in the measurements, since the temperature difference between the hot wall and the interface is only 1.1 or 2.1°C. For example, the consistent upturn in temperatures in the middle of the melt is within the experimental uncertainty.

Comparison between predictions and experimental data

Comparisons between numerical predictions and experimental results are made for one experiment: $T_i = 233.0°C$, $T_H = 233.0°C$, $T_C = 229.0°C$, $Ra = 1.59 \times 10^5$, $Ste = 1.32 \times 10^{-2}$, $Pr = 0.011$ and $A = 0.75$. The calculations are performed on a CYBER 205 digital computer. The total simulated dimensionless time is $\tau = 0.16$ (numerically determined steady state). Because of the very large computational costs (2.55×10^4 CPU s), only one simulation is performed. Computational time is excessive owing to very slow convergence for low Prandtl number fluids.

Figure 10 shows velocity vector maps at preselected times for the simulation of one experiment (Fig. 5). A large, clockwise rotating convection cell develops early (Fig. 10(a)) and decreases in size as solidification progresses (Figs. 10(b) and (c)). In the center of the recirculation eddy, the velocities are as much as one order of magnitude lower than the ones in the boundary layers. Small secondary recirculation cells are observed in the corners of the liquid filled pool (Fig. 10(a)). At these locations the main flow separates from the sidewalls and makes a 90° turn. Due to the secondary recirculation cells, the impingement of the main flow does not occur in the immediate vicinity of the corners, but is vertically and horizontally shifted at the heated sidewall, solid–liquid interface and top and bottom wall, respectively. As solidification progresses (Figs. 10(b) and (c)), the two, initially small recirculation cells at the bottom have grown together to one large recirculation region which comprises several small convection cells. Even though the secondary eddy at the top of the solid–liquid interface is small in size, it significantly influences the local heat transfer at the interface. The minimum local solidification rate is not at the top of the cavity, but in the region where the main flow impinges on the interface.

Figure 11 shows predicted and measured interface positions. The symbols and the solid lines represent the experimental data and the predictions at preselected times, respectively. At early times ($t = 0.077$ h) the numerical model overpredicts the solidified volume. The discrepancy may be partly attributed to supercooling and to thermal inertia of the experimental apparatus. Due to the thermal inertia of the experimental setup, it is impossible to impulsively lower the temperature at one vertical wall in order to initiate the solidification process. This instantaneous change in the wall temperature is one of the assumptions made in the numerical model. In the experiment, approximately 2 min (1.75% of the total experimental time) elapse before the desired temperature at the cold wall is reached. During this period of time, the temperature difference ($T_f - T_C$) and thus the driving potential for solidification, is smaller than the one used in the numerical simulation which is based on the desired cold-wall temperature. This causes the overprediction of the solidified volume at early times ($t = 0.077$ h).

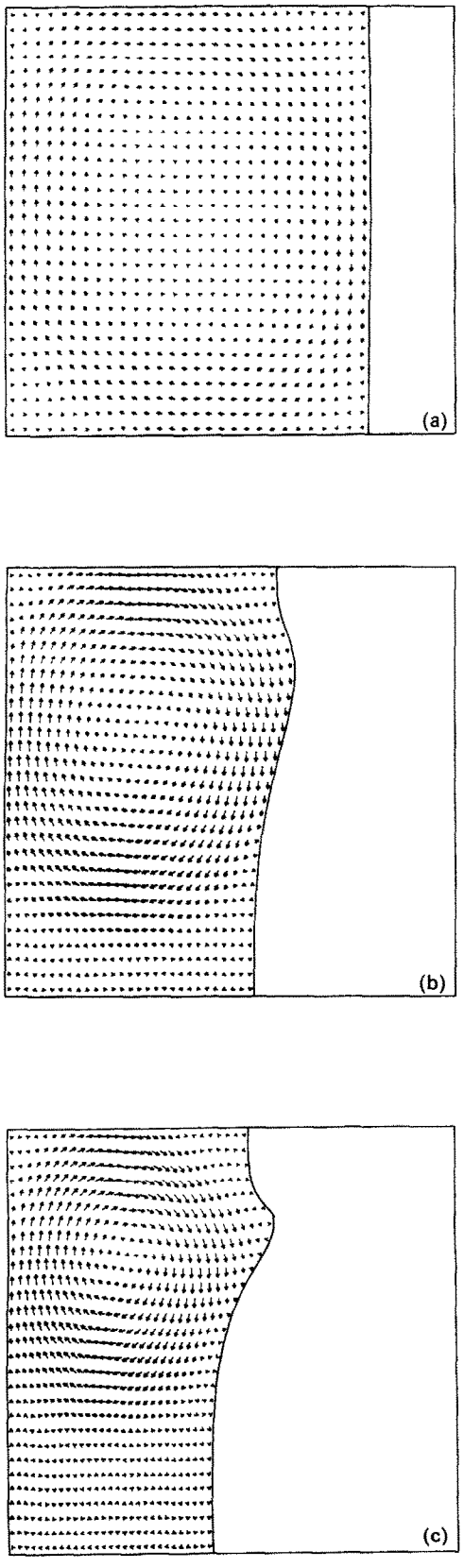

FIG. 10. Velocity vector map for $T_i = 233.0$°C, $T_H = 233.0$°C, $T_C = 229.0$°C, $A = 0.75$, $Ra = 1.59 \times 10^5$, $Ste = 1.32 \times 10^{-2}$: (a) $t = 0.079$ h ($Fo = 0.63$); (b) $t = 0.529$ h ($Fo = 4.31$); (c) $t = 1.486$ h ($Fo = 12.11$).

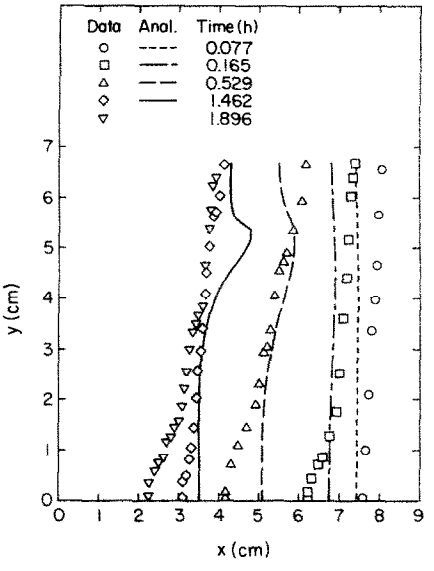

FIG. 11. Comparison between measured and predicted interface locations at preselected times: $T_i = 233.0$ C, $T_H = 233.0$°C, $T_C = 229.0$°C, $A = 0.75$, $Ra = 1.59 \times 10^5$, $Ste = 1.32 \times 10^{-2}$.

As solidification progresses, the discrepancy between the experimental data and the predictions becomes smaller, and after $t = 0.529$ h the experimentally determined solidified volume is larger than the predicted one. Lower hot- and cold-wall temperatures during the experiment at later times than the ones used in the numerical simulation as well as heat losses from the test cell to the ambient may contribute to higher measured than predicted solidification rates. At $t = 1.462$ h the comparison between the experimental data and predictions is quite disappointing. While the lowest local solidification rate is measured at the top of the wall, the predicted local minimum occurs at about $x/H = 0.8$. This is attributed primarily to the difference between the predicted and actual flow structures in the melt. Shrinkage of the solid and motion of the liquid away from the upper connecting wall due to the solidification of tin (because $\rho_s > \rho_l$), and insufficient resolution due to the coarse numerical grid are believed to be the main causes for the difference. The unavoidable shrinkage causes a change in the velocity boundary condition from one of no slip (equation (6)) to one of no shear and in the process is expected to change the flow structure in the upper part of the melt region. Steady-state natural convection calculations in liquid metals ($Pr \cong 0.01$) have revealed secondary cells in the four corners of a rectangular cavity [14], but such cells have not been predicted in ordinary fluids [13]. It is unfortunate that metals are opaque to visible radiation and hence do not allow for flow visualization. Attempts to measure the velocity near a vertical wall with an incorporated magnetic probe [15] provided by Professor Vivès were unsuccessful, apparently because the velocities under natural convection conditions in a small test cell were too small and/or

temperature gradients were possibly too large and had not been properly calibrated.

Additional factors which may contribute to the discrepancy between data and predictions include possible crystallographic effects at the solidification front [2], unavoidable heat losses from the bottom of the test cell, neglect of the density difference between the solid and the liquid phases and of the finite velocity at the solidification front. Even though the last effect can be accounted for in the analysis [16], estimates show that for the conditions studied it is not significant. All of these factors can affect the flow structure in the melt and alter the solidification front shape and its motion.

Temperature profiles measured for three different heights at preselected times and predictions are shown in Fig. 12. Again, the experimental data are denoted with symbols, and the numerical results are shown with a solid line. While there is scatter in the experimental results, the measured and predicted temperature distributions agree qualitatively. Some of the discrepancies can be attributed to heat losses from the test cell and measurement errors as well as computational inaccuracies.

CONCLUSIONS

A combined experimental and numerical study of solidification of pure tin at a vertical wall in the presence of liquid superheat is performed. Temperature and interface position measurements have been used to deduce the importance of natural convection in the liquid pool on the solidification process. However, since the thermal conductivity of tin is two orders of magnitude higher than the ones of ordinary liquids, the effects of natural convection on the shape and motion of the solid–liquid interface is not as large as during phase-change heat transfer of non-metallic substances.

A comparison between experimental temperature data and numerical predictions shows good agreement, while there is some scatter in the experimentally measured temperatures. The correspondence between measured and predicted interface positions is only fair and in some ways disappointing. Differences between the measured and predicted interface shapes suggest different flow structures near the interface during the experiment than it has been predicted numerically, primarily because of the idealizations in the mathematical model and possibly as a result of too coarse a numerical grid.

The calculations have indicated a clear need for a much more efficient algorithm to solve multidimensional transport equations describing solidification of metals and metal alloys in which flow of the melt must be accounted for. In addition, there is a need for computational schemes which are capable of tracking simultaneously several moving boundaries (e.g. solid–liquid, solid–gas and liquid–gas) that occur when a material shrinks upon solidification.

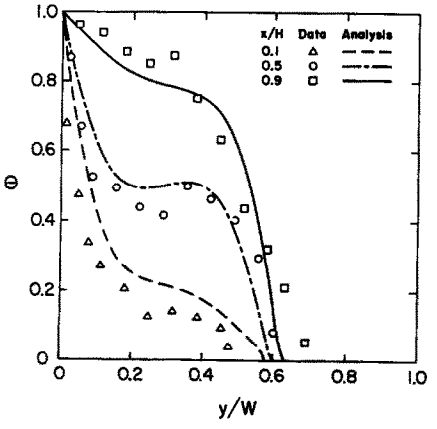

FIG. 12. Comparison between measured and predicted temperature distributions at three different heights: $T_i = 233.0°C$, $T_H = 233.0°C$, $T_C = 229.0°C$, $A = 0.75$, $Ra = 1.59 \times 10^5$, $Ste = 1.32 \times 10^{-2}$, $t = 0.529$ h ($Fo = 4.31$).

Acknowledgements—This research was supported, in part, by the National Science Foundation under Grant No. CBT-8313573. The computing facilities were made available by Purdue University Computing Center.

REFERENCES

1. M. J. Stewart and F. Weinberg, Fluid flow in liquid metals: 2. Experimental observations, *J. Crystal Growth* **12**, 228–238 (1971).
2. C. Gau and R. Viskanta, Melting and solidification of a pure metal on a vertical wall, *J. Heat Transfer* **108**, 174–181 (1986).
3. A. W. D. Hills, S. L. Malhotra and M. R. Moore, The solidification of pure metals under unidirectional heat flow condition: II. Solidification in the presence of superheat, *Met. Trans.* **6B**, 131–142 (1975).
4. J. Szekely and P. S. Chhabra, The effect of natural convection on the shape and movement of the melt–solid interface in the controlled solidification, *Met. Trans.* **B1**, 1195–1203 (1970).
5. C. Vivès and C. Perry, Solidification of a pure metal in the presence of a stationary magnetic field, *Int. Commun. Heat Mass Transfer* **13**, 253–263 (1986).
6. C. Vives and C. Perry, Effects of electromagnetic stirring during the controlled solidification of tin, *Int. J. Heat Mass Transfer* **29**, 21–23 (1986).
7. N. Ramachandran, J. P. Gupta and Y. Jaluria, Thermal and fluid flow effects during solidification in a rectangular enclosure, *Int. J. Heat Mass Transfer* **25**, 187–194 (1982).
8. M. Flemings, *Solidification Processing*. McGraw-Hill, New York (1974).
9. S. Ostrach, Fluid mechanics in crystal growth—The 1982 Freeman Scholar Lecture, *J. Fluid Engng* **105**, 5–20 (1983).
10. E. S. Hedges, *Tin and its Alloys*. Edward Arnold, London (1960).
11. W. H. Cubberly, *Metal Handbook, Properties and Selection: Nonferrous Alloys and Pure Metals*, 9th Edn. ASM, Metal Park, Ohio (1979).
12. M. Ozisik, *Heat Conduction*, pp. 399–435. Wiley, New York (1980).
13. G. DeVahl Davis, Natural convection of air in a square cavity: a benchmark numerical solution, *Int. J. Numer. Meth. Fluids* **3**, 249–264 (1983).

14. F. Wolff, C. Beckermann and R. Viskanta, Natural convection of liquid metals in vertical cavities, *Expl Thermal Fluid Sci.* (1988), in press.
15. R. Ricou and C. Vives, Local velocity and mass transfer measurements in molten metals using an incorporated magnetic probe, *Int. J. Heat Mass Transfer* **25,** 1579–1588 (1982).
16. E. M. Sparrow, S. V. Patankar and S. Ramadhyani, Analysis of melting in the presence of natural convection in the melt region, *J. Heat Transfer* **99,** 520–526 (1977).

SOLIDIFICATION D'UN METAL PUR A UNE PAROI VERTICALE EN PRESENCE D'UN LIQUIDE SURCHAUFFE

Résumé—La rôle de la convection naturelle pendant la solidification d'un métal pur à une paroi verticale est étudié expérimentalement et numériquement. Des expériences sont conduites dans une cellule d'essai rectangulaire ayant deux parois opposées tenues à des températures constantes mais différentes, alors que les autres parois sont bien isolées. De l'étain pur est utilisé comme matériau à changement de phase. Des mesures de température et de position de l'interface solide–liquide dans des conditions contrôlées avec soin, sont utilisées pour déduire l'importance de la convection naturelle, dans le métal liquide, sur la distribution de température dans le bain aussi bien que sur la forme et le mouvement de l'interface solide–liquide. Les données expérimentales sont comparées avec les résultats d'une prédiction numériques.

ERSTARREN EINES REINEN METALLS AN EINER VERTIKALEN WAND BEI ÜBERHITZTER SCHMELZE

Zusammenfassung—Der Einfluß der natürlichen Konvektion bei der Erstarrung eines reinen Metalls an einer vertikalen Wand wird experimentell und numerisch untersucht. Es werden Experimente in einer rechtwinkligen Testzelle durchgeführt, bei der zwei gegenüberliegende Wände auf verschiedenen, aber jeweils konstanten Temperaturen gehalten werden, während die übrigen Wände gut wärmegedämmt sind. Es wird reines Zinn benutzt. Temperaturen und die Position der Grenzfläche zwischen verfestigtem und flüssigem Metall werden gemessen, um den Einfluß der natürlichen Konvektion auf die Temperaturverteilung der Schmelze und auf die Form und Bewegung der Grenzfläche zu ermitteln. Die experimentellen Resultate werden mit Ergebnissen von numerischen Berechnungen verglichen.

ЗАТВЕРДЕВАНИЕ ЧИСТОГО МЕТАЛЛА НА ВЕРТИКАЛЬНОЙ СТЕНКЕ ПРИ ПЕРЕГРЕВЕ ЖИДКОСТИ

Аннотация—Экспериментально и численно исследовалась роль естественной конвекции при затвердевании чистого металла на вертикальной стенке. Эксперименты проводились в прямоугольной ячейке, в которой две противоположные стенки имели постоянную, но различную температуру, а две другие были хорошо изолированы. В качестве рабочего материала использовалось чистое олово. Измеренные значения температуры и положения границы раздела фаз твердое тело–жидкость, выполненные в строго контролируемых условиях, использовались для выяснения влияния естественной конвекции в жидком металле на распределения температуры в расплаве, а также на форму и движение границы раздела. Проведено сравнение экспериментальных данных с результатами численных расчетов.